PREDICTION OF DISPLACEMENTS IN TUNNELS

N. Radončić[1] T. Pilgerstorfer[1] and Wulf Schubert[1]

[1]*Insitute for Rock Mechanics and Tunnelling*
Graz University of Technology, Austria
(nedim.radoncic@tugraz.at)

Abstract

One of the major drawbacks of two-dimensional approaches in underground excavation design is the (mostly) inadequate modelling of the effects of the face advance. The amount of pre-displacements and the evolution of the displacements towards their final value are generally roughly estimated. On the other hand, 3D calculations pose a much greater modelling and evaluation challenge, and can be conducted only by the usage of numerical methods.

The work presented in this publication is directed towards narrowing of this gap. It concerns the determination of the displacement evolution in an elasto-plastic, Mohr-Coulomb medium under hydrostatic primary stress state. 3D numerical simulations with FLAC 3D have been used to generate the displacement evolutions for various parameter combinations. The parameters have been chosen in such way that they form a regular grid in a co-ordinate system spanned by the friction angle and a unit-less variable defined as the ratio between the depth of failure and the tunnel radius. Utilizing the closed-form solution by Feder and Arwanitakis, the equivalent fictitious support pressure was calculated from the provided displacement paths, thus allowing the establishment of three interpolation relationships. The development of the fictitious support pressure can be directly derived from these interpolation relationships, hence predicting both the displacement development and the amount of pre-relaxation of the ground.

The effects of lining installation can be easily incorporated in this model by superposing the fictitious support pressure with the mobilized support pressure, while obeying the displacement compatibility between the liner and the rock mass. Both the solution scheme and its validation are presented in this paper, together with an empirical relationship depicting the rheological properties of shotcrete. The combination of these relationships enables an approximate estimation of the displacement development with installed shotcrete support and of the associated shotcrete utilisation ratio, hence allowing very fast assessment of the system behaviour in given tunnelling conditions.

The results obtained with the application of the presented method are discussed, depicting selected tunnelling scenarios and their impact on the lining displacement development and associated utilisation ratio.

Keywords: shotcrete; shotcrete utilisation; advance rate; displacement development, support design

1. Introduction

When tunnelling in difficult ground conditions, the importance of the ability to correctly predict the magnitude, spatial orientation and development path of the displacements caused by the excavation and associated stress re-distribution cannot be overstressed. The entire scope of displacement information, as stated above, can be *a priori* predicted only by numerical methods. However, the prediction of radial displacement magnitude and its path towards final convergence are also possible with closed-form solutions and different empirical relationships [1,2,3]. Since the displacements in the plane perpendicular to the tunnel axis have the highest magnitude and result in the highest loading of the lining, this work omits the longitudinal displacements completely.

The method presented in this paper represents an easy-to-implement tool allowing fast assessment of displacement development for a circular cavity in a linearly elastic - ideally plastic Mohr-Coulomb material under hydrostatic loading, also incorporating the aspects of ongoing hydration, shrinkage and creep of the shotcrete lining. Its application should allow the engineer to assess the system behaviour and chose a technically feasible design before starting more complex numerical calculations.

1.1. *State of the art*

The simple empirical relationship (Eqn. 1) developed by Sulem, Panet & Guenot [3] incorporates the effect of the face advance on the development of the displacements.

$$C_1(x) = C_{\infty x} \cdot \left[1 - \left(\frac{X}{x + X} \right)^2 \right] \quad (1)$$

Where:

$C_1(x)$	Radial displacement at the relative distance to face x
$C_{\infty x}$	Final radial displacement (infinite face distance)
X	parameter of the convergence law
x	distance to the face

It fits both on-site measured displacements [4] and numerical results very well. Panet & Guenot [2] incorporated a relationship between the development of the displacements and the radius of the plastic zone (Eqn. 2).

$$u(x) = u_f + (u_\infty - u_f) \cdot \left[1 - \left(\frac{0.84 \cdot R_p}{x + 0.84 \cdot R_p} \right)^2 \right] \quad (2)$$

Where:

$u(x)$	Radial displacement at the relative distance to face x
u_∞	Final radial displacement (infinite face distance)
u_f	Radial displacement at the face (x=0)
R_p	Radius of the plastic zone

Hence, if the displacement magnitude at the face, the final displacement and the extent of the plastic zone are known, the displacement development can be predicted. The displacement developments obtained from the application of the above relationship and the closed-form solution by Feder & Arwanitakis [5] have been compared to the results of 3D numerical simulations and show excellent predictive quality.

If used in combination with the convergence confinement method and simple, linearly elastic – ideally plastic material laws for the installed lining, the equation 2 yields very satisfying results [1]. The drawback lies in the prediction of the displacement development on the basis of the final convergence and plastic radius, hence making the incorporation of a more complex, time-dependant support characteristic almost impossible.

2. Prediction of the fictitious support pressure development

In order to circumvent the drawbacks mentioned above, a numerical parametric study on a 3D model in FLAC3D has been conducted. The goal was the establishment of an empirical set of equations based on work of Sulem, Panet and Guenot predicting the development of a "fictitious support pressure". The fictitious support pressure has been defined as a support pressure having to be applied in the closed-form solution in order to obtain the displacement equal to the displacement obtained from the 3D model at the respective face distance. The parameters controlling the shape of the fictitious support pressure development curve have been determined for data obtained from every numerical simulation, thus creating a basis for a set of surfaces interpolating the curve parameter values.

2.1. *Parametric study*

The study was performed within a wide span of material parameters. The requirement of broad applicability made it necessary to establish a general dimensionless relationship between the strength parameters and the primary stress state. This was solved by establishing the variable η, defined as the ratio between the depth of failure $d_{failure}$ and the radius of the tunnel R (Eqn. 3).

$$\eta = \frac{d_{failure}}{R} \quad (3)$$

The establishment of the relative depth of the failure zone removes the primary stress

magnitude as an input parameter, since it is implicitly represented by the depth of failure. Since there is an infinite number of combinations of cohesion and friction angle leading to the same depth of failure under a constant primary stress magnitude, the friction angle was subsequently fixed to values of 20, 30 and 40 degrees (Figure 1). The associated cohesion has been chosen in such way that the variable η spans the range between 0 (elastic solution) and 2,5 (the plastic radius is 3,5 times higher then the tunnel radius). The primary stress state equalled 20 MPa in all calculations.

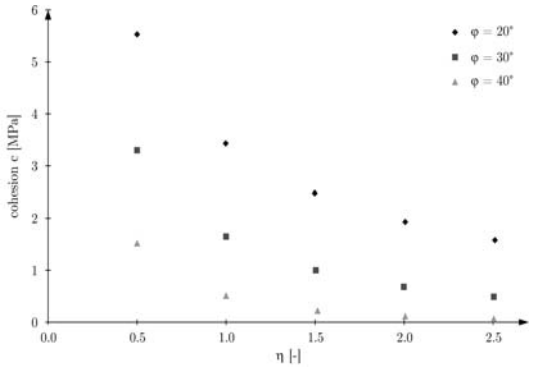

Figure 1: the relationship between the Mohr-Coulomb strength parameters and the relative depth of the failure zone

The determination of the fictitious support pressure has shown that the elastic parameters E and v have no influence on it. These parameters are of tremendous importance for the development of absolute displacements, but the fictitious support pressure, as defined above, is always the same if the given face position, strength parameters and primary stress state are kept constant.

2.2. *Calculation of the fictitious support pressure*

Based on the displacement data obtained from the numerical calculations, the respective fictitious support pressures $\widetilde{p}_i$ have been calculated for every relative face position x using the closed-form solution by Feder & Arwanitakis [5] (Figure 2).

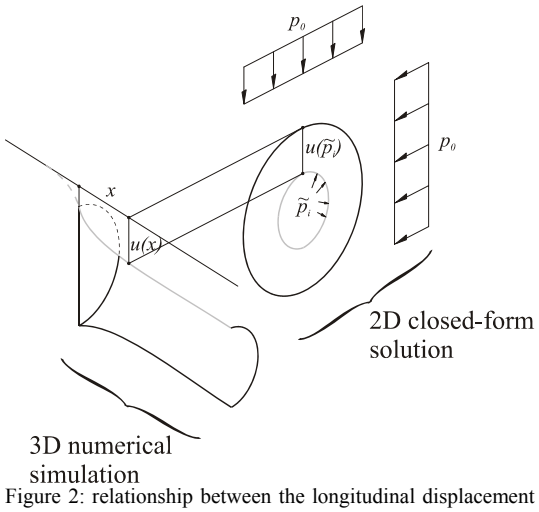

Figure 2: relationship between the longitudinal displacement profile from the 3D numerical model, radial displacement obtained from the 2D closed-from solution and fictitious support pressure

The series of equivalent support pressures thus obtained has been converted to their dimensionless form λ, called equivalent support pressure coefficient in further text, and defined as the ratio between the fictitious support pressure and the primary stress (Eqn. 4) .

$$\lambda = \frac{\widetilde{p}_i}{p_0} \qquad (4)$$

The geometric influence of tunnel size on the displacement development is removed by normalizing the face distance x with the influence length L_{infl}, defined as the face distance required for the displacements to reach 99% of their final convergence.

After both of the above transformations have been performed, the obtained unitless data has been fitted with a slightly modified version of the function after Sulem et al. (Eqn. 5).

$$\lambda(x) = \lambda_{face} \cdot \xi^{1.2} \cdot \left(\frac{1-x}{x+\xi} \right)^{1.2} \qquad (5)$$

It has been found that the above relationship fits the equivalent support pressure coefficient data very well (Figure 3).

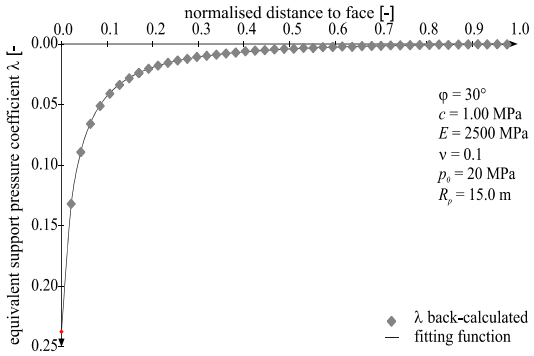

Figure 3: comparison equivalent support pressure coefficient obtained from the numerical calculation and the fitting function

Hence, the development of the equivalent support pressure coefficient is described by three function shape parameters: λ_{face}, ξ and L_{infl}.

2.3. *Shape parameter interpolation*

The results of the numerical calculations with the parameters presented in chapter 2.1 have been fitted with the function described by the Eqn. 5, hence obtaining the shape parameters throughout the entire material parameter range. Based on these discrete points, three interpolation relationships have been established.

2.3.1. *Influence length*

The influence length is almost invariant with regard to the friction angle and features almost linear dependency with the depth of the failure zone (Figure 4).

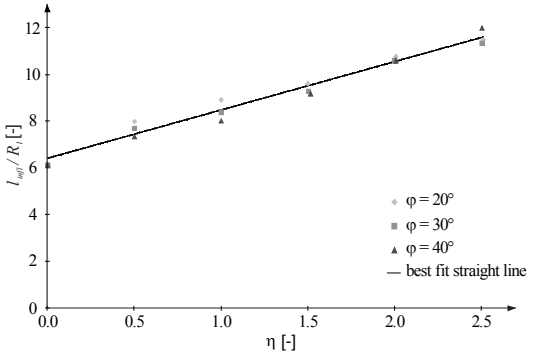

Figure 4: the simulation results and the applied fitting relationship

The linear relationship presented herein writes as:

$$L_{Infl} = (2.07 \cdot \eta + 6.40) \cdot R \qquad (6)$$

The invariance towards friction angle is consistent with the Equation 2, stating that the displacement development is influenced solely by the radius of the plastic zone (implicitly represented by η in this case).

2.3.2. *Pre-relaxation coefficient λ_{face}*

The values of the pre-relaxation coefficient λ_{face} yield a mechanically plausible pattern when plotted spatially, with x and y axis representing the relative depth of failure η and the friction angle, respectively. The interpolation surface writes as

$$\lambda_{face} = a \cdot cos(b \cdot \eta + c) + d \cdot \eta + e \qquad (7)$$

wherein

$$a = 0.1314 \cdot tan(\varphi) + 0.0129$$
$$b = -0.0259 \cdot tan(\varphi) + 2.6227$$
$$c = 0.011 \cdot tan(\varphi) - 0.6439$$
$$d = -0.1854 \cdot tan(\varphi) - 0.1593$$
$$e = -0.1396 \cdot tan(\varphi) + 0.8092$$

The interpolation surface defined by this equation is represented in Figure 5.

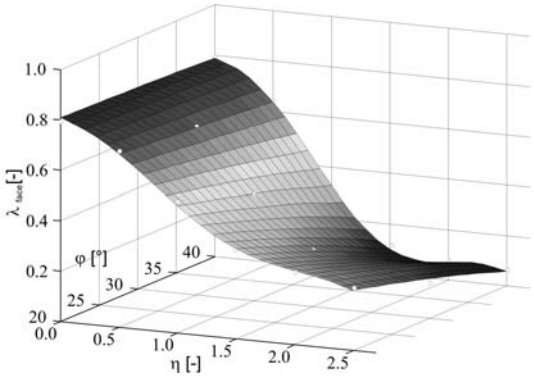

Figure 5: the discrete pre-relaxation data obtained from the numerical calculations and the interpolation surface fitting it

At this point it has to be stressed that this finding is of considerable importance: when performing 2D calculations and applying the load reduction method, the usual amount of pre-relaxation is

assumed to equal 0.3, implying that the pre-relaxation is directly proportional to the amount of the usually assessed amount of pre-displacements. While the findings of this study confirm that the amount of pre-displacements in unsupported case equals 0,25 to 0,3 of the total displacements, the amount of pre-relaxation is *vastly* different. For relatively high plastic radii (η equals 2,5) and high friction angles, the fictitious support pressure at the tunnel face equals merely 10% of the primary stress magnitude.

2.3.3. *Shape parameter ξ*

Similar to the aforementioned trend established for the pre-relaxation coefficient, the shape parameter ξ interpolation relationship has been established by plotting the discrete data in the co-ordinate system spanned by η and the friction angle (Figure 6).

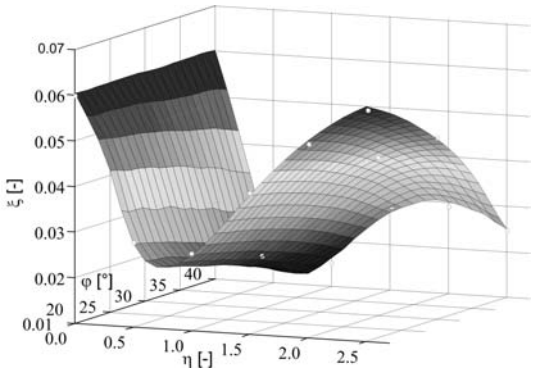

Figure 6: discrete data points for the shape parameter ξ obtained from the numerical simulations and the interpolation surface fitting it

On the contrary to the other two parameters, this parameter does not have any physical meaning: it simply controls the shape of the function predicting the equivalent support pressure coefficient. The interpolation relationship is given by:

$$\xi = \bar{a} \cdot cos(\bar{b} \cdot \sqrt{\eta} - \eta + \bar{c}) + \bar{d} + \bar{e} \cdot \eta \qquad (8)$$

Wherein

$$\bar{a} = 0.023625$$

$$\bar{b} = 0.4604 \cdot tan^2(\varphi) + 0.3749 \cdot tan(\varphi) ... \\ ... + 5.5276$$

$$\bar{c} = -0.0397 \cdot tan^2(\varphi) + 0.015 \cdot tan(\varphi) ... \\ ... - 1.0327$$

$$d = -0.1854 \cdot tan(\varphi) - 0{,}1593$$

$$\bar{e} = -0.0247 \cdot tan^2(\varphi) - 0.006 \cdot tan(\varphi) ... \\ ... + 0.0039$$

2.4. *Application procedure*

The application procedure for the presented set of equations is straightforward:

(i) Calculate the plastic radius and the associated relative depth of failure η from the given primary stress state and strength parameters of the ground*;*
(ii) Estimate the influence length L_{infl};
(iii) Estimate the pre-relaxation coefficient λ_{face} from the respective interpolation relationship;
(iv) Estimate the shape parameter ξ from the respective interpolation relationship;
(v) For every positive face distance x (therefore, after the excavation has passed the cross-section under consideration) calculate the equivalent support pressure coefficient $\lambda(x)$;
(vi) From every support pressure coefficient $\lambda(x)$ and the primary stress state, calculate the fictitious support pressure $p_i(x)$*;*
(vii) Using the closed-form solution by Feder & Arwanitakis [5], calculate the radial displacement by considering the fictitious support pressure for every face distance x under consideration.

3. Incorporating lining support

The effect of passive support is considered by a very simple idea: the support pressure activated by imposing the radial deformations on the lining can be added to the fictitious support pressure in order to obtain the displacement development in case of an installed lining (Figure 7). Since the excavation boundary and the lining boundary are forced to experience the same amount of radial displacements (displacement compatibility) the

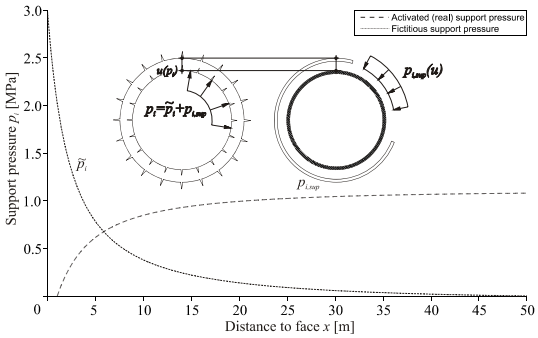

Figure 7: superposition of the fictitious and the "mobilized" support pressure activated by displacements forced upon the lining (lining installation 1 m behind the tunnel face)

problem can be solved by formulating it as a function and finding its root. Assuming that the installed liner is linear elastic, with the Young's modulus E and thickness t, the radial stiffness of the lining calculates as

$$K_{Lining} = \frac{t \cdot E}{R^2} \quad (9)$$

thus allowing the calculation of the "mobilized" support pressure as

$$p_{a,sup} = u \cdot K_{Lining} \quad (10)$$

wherein u represents the radial deformation of the lining. Since the closed-form solutions generally yield total displacements, the amount of pre-displacements u_{pre} calculated by inserting the fictitious support pressure corresponding to the face position where the lining is being installed, must be subtracted (Eqn. 11) from the total displacements. Simply put, the displacements happening *before* the liner has been installed do not interact with it and do not result in any loading.

$$u = u_{tot} - u_{pre} \quad (11)$$

If the function $S(p_i)$ yields the displacements obtained from the closed form solution (the other input parameters as primary stress state and ground properties are kept constant) depending solely on the support pressure, the out-of-equilibrium radial stress at the excavation-liner boundary $\sigma_{r,err}$ writes as:

$$\sigma_{r,err} = p_{i,sup} - K \cdot S\left(\tilde{p}_i + p_{i,sup}\right) \quad (12)$$

The root of this relationship represents the force equilibrium and the sought-for problem solution – the radial displacements obtained at this state represent approximately the displacements accounting for the effect of support installation. In the course of this work, Newton's root-finding algorhitm was used and proved to be very fast and features stable convergence behaviour. The required derivative of the function was calculated by numerical means, using a finite difference with a very small perturbation width. The equilibrium finding procedure has to be found for every respective face position, since the fictitious support pressure changes with every excavation step.

3.1. *Method verification*

In order to verify the results of the method presented here, a set of FLAC3D calculations has been conducted, with various lining stiffness parameters and distances between face and lining installation. The lining was modelled with structural elements of the membrane type, allowing normal force loading but no bending moments. Lining's Young's modulus equalled 2000 MPa (which approximately models the stiffness of the shotcrete lining subjected to normal loading rates, creep and shrinkage effects) and the distance between the face and lining installation was set to 1m. The results show that the method presented here tends to overestimate the displacements (Figure 8).

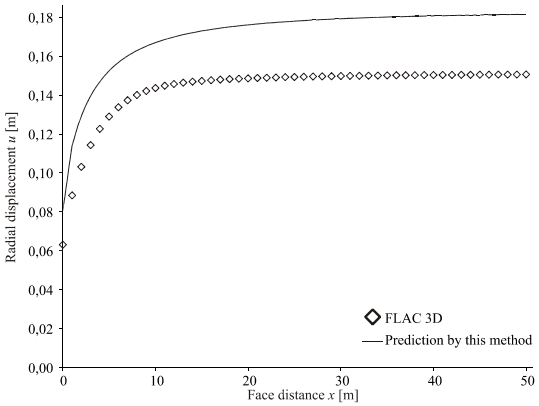

Figure 8: comparison between numerical results and the results of the presented analytical method

The reasons for this discrepancy lie in the boundary truncation effects of the numerical model, and the additional loading of the lining due to longitudinal stress redistribution and its interaction with the lining. However, since the presented method was developed in order to allow a fast assessment of system behaviour, this drawback and the presented error have been deemed acceptable. It has to be stated that the work on method verification has yielded highly unsatisfactory results in cases of very stiff support (e.g. pre-cast concrete segments) installed very closely to the face, so great attention should be paid to results of analysis in similar conditions.

4. Rheological behaviour of shotcrete

In order to depict the influence of the time- and load-dependent mechanical properties of shotcrete on the general system behaviour, the flow-rate method as proposed by Schubert [6] has been implemented in the algorithm presented above. It assumes that the strain of shotcrete subjected to loading is composed of 4 components:

(i) Immediate, elastic deformation, proportional to the applied stress and to the respective, time-dependent Young's modulus;
(ii) Reversible creep deformation;
(iii) Irreversible creep deformation, dependant on the age and on the loading history of shotcrete;
(iv) Isotropic shrinkage and temperature deformation.

Calculation of shotcrete stress is possible if the shotcrete strains ε_1 and ε_2, the time information t for every deformation increment and the stress history σ_1 (up to the respective moment) are known (Eqn. 13).

$$\sigma_2 = \frac{\varepsilon_2 - \varepsilon_1 + \frac{\sigma_1}{E(t)} + \varepsilon_d\left\{1 - e^{-\Delta C(t)/Q}\right\} - \Delta\varepsilon_{sh}}{\frac{1}{E(t)} + \Delta C(t) + C_{d\infty}\left(1 - e^{-\Delta C(t)/Q}\right)} \quad \ldots\ldots\ldots\ldots\ldots\ldots\ldots\ldots\ldots\ldots \quad (13)$$

The plastic, non-reversible creep evolution is defined as

$$C(t) = At^{1/3} \quad (14)$$

Hence enabling the calculation of the increment $\Delta C(t)$ as follows:

$$\Delta C(t) = A\left(t_2^{1/3} - t_1^{1/3}\right) \quad (15)$$

The evolution of the Young's modulus due to hydration of shotcrete is defined as:

$$E(t) = E_{28}\left[(4{,}2 + 0{,}85t)/t\right]^{-0{,}3} \quad (16)$$

The creep strain increment is calculated by the following equation:

$$\Delta\varepsilon_d = (\sigma_1 C_d - \varepsilon_d)(1 - e^{\frac{-\Delta C(t)}{Q}}) \quad (17)$$

The constants C_d and Q are material parameters and the variable ε_d is defined as the sum of creep strain increments:

$$\varepsilon_d = \sum \Delta\varepsilon_{d,i} \quad (18)$$

The shrinkage strain writes as

$$\varepsilon_{sh} = \frac{\varepsilon_{sh\infty} \cdot t}{B + t} \quad (19)$$

wherein B represents a material parameter, t is the shotcrete age in days and $\varepsilon_{sh\infty}$ is the final shrinkage strain. The parameters used in the following calculations are presented in the following table:

Table 1: parameter values of the rheological shotcrete model

Parameter	Value
E_{28}	16000
A	0.00025
C_d	0.000214
Q	0.0000221
B	10
$\varepsilon_{sh\infty}$	0.000974

The shotcrete parameters above represent only an assessment of shotcrete properties. The test set-up and the methods allowing their determination from on-site shotcrete testing have been presented in [7] and will not be discussed further in the course of this work.

4.1. *Combination with the displacement-predicting algorithm*

The Equation 13 predicts the tangential stresses in the lining on the basis of radial strains, time information and loading history. Hence, the presented set of relationships has only to be modified in such way that the lining behaviour is not assumed as not being linearly elastic:

$$\sigma_{r,err} = p_{i,sup} - p_{i,sup\,shot}(u,t,\sigma) \qquad (20)$$

Wherein $p_{i,sup,shot}(u,t,\sigma)$ represents the mobilized support pressure calculated by the application of the flow-rate method. The solution procedure is the same as in the first example. Additional information regarding tunnel advance (time-face position data), stresses from past calculation steps and strains from past calculation steps have to be provided to the algorithm.

4.2. *Shotcrete utilisation ratio*

The shotcrete utilisation ratio is defined as a ratio between current shotcrete stress $\sigma_{shotcrete}(t)$ and its currently (due to hydration) available load capacity $\sigma_{shot,max}(t)$:

$$\beta(t) = \frac{\sigma_{shotcrete}(t)}{\sigma_{shot,max}(t)} \qquad (21)$$

It is hence a unitless variable, with values above 1 indicating failure of the tunnel lining. The relationship describing the evolution of the shotcrete compressive strength $\sigma_{shot,max}(t)$ has been taken over from Eurocode 2 [8].

5. Results

In order to illustrate the predictive ability and importance of the method presented above, two case-studies have been performed. The first one shows the influence of the tunnel advance rate on the shotcrete stresses and the associated utilisation ratio, and the second one depicts the effects of a construction stop and re-start after considerable time.

5.1. *Tunnel advance rate*

Both calculations have been performed with Mohr-Coulomb ground parameters of φ = 30°, c = 0.50 MPa, Young's modulus of 2500 MPa and Poisson's ratio of 0.1, with the primary stress equalling 15 MPa. The shotcrete support was installed 2 m after the face, and the examined advance rates were 3.5 and 5.0 meters on day. The results show a drastic difference in the utilisation ratio: the faster tunnel advance results in much higher strain increments, with shotcrete having almost no time for curing and developing strength (Figure 9).

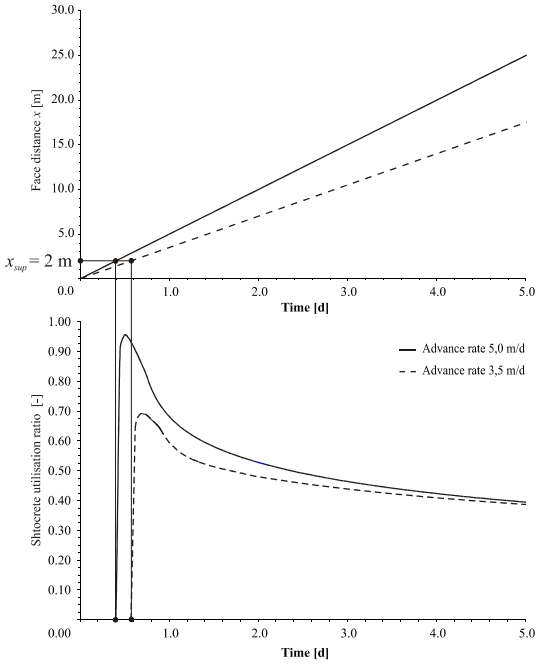

Figure 9: comparison between two cases of tunnelling in the ground with same ground properties and support concepts but different advance rates

However, since the creep of young shotcrete is highly dependent on the load history, the shotcrete loading level in the case of fast advance quickly decreases from the initial peak of 0.95 towards the value of 0.50 in the following 4 days.

5.2. *Construction stop and re-assuming the advance*

In this case, we assume that the tunnel advance rate is constant at 3.0 m/d, then there is a construction stop for 5 days, and then the

heading is re-assumed with the rate of 5.0 m/d (Figure 10).

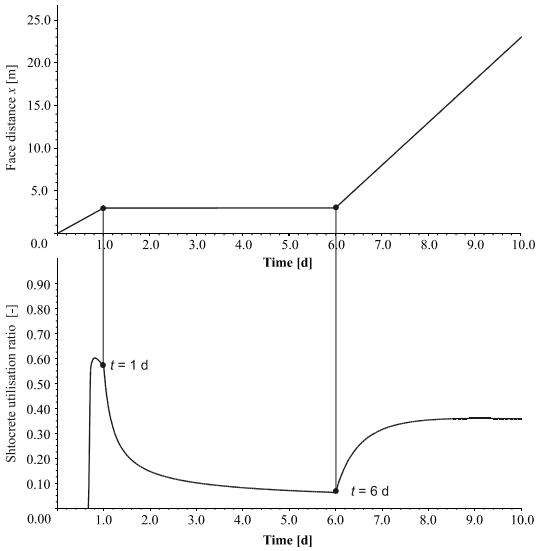

Figure 10: comparison between two cases of tunnelling in the ground with same ground properties and support concepts but different advance rates

The shotcrete utilisation raises to considerable levels after the excavation is reassumed, in spite of the continuously increasing shotcrete strength. There are two main reasons for this effect: the Young's modulus of the shotcrete is increasing with the ongoing hydration as well, and the ability of shotcrete to dissipate high stresses by creep is continuously decreasing. Hence, the shotcrete lining has a much higher stiffness after the excavation is re-started.

This effect has been observed in practice as well, and the usual way of dealing with the sudden stress increase after a prolonged construction stop is the strengthening of the respective cross section by an increased number of rock bolts and an increase in lining thickness (helps only up to a certain degree). It has to be noted that this mechanism becomes relevant only for support near to the tunnel face, since the displacement increments after re-starting the excavation are highest in this area.

6. Conclusion

This paper presents a novel method predicting the pre-relaxation and displacement development for a circular cavity in a hydrostatically loaded ground. It allows, if the information about the face advance rate is provided, a quick and sound assessment of the lining stresses while incorporating the effects of shotcrete creep, shrinkage and curing.

The shortcomings of the method are clear as well: the softening behaviour of the ground (if present), the longitudinal displacements, the effects of sequential excavation and arbitrary primary stress states are not accounted for.

On the other hand, this method was not developed as a replacement for numerical methods, but as a rough tool allowing plausibility checks and model calibration before more complex calculations are performed.

1 Carranza-Torres, C. & C. Fairhurst 1999. *Application of the Convergence Confinement Method of Tunnel Design to Rock Masses That Satisfy the Hoek-Brown Failure Criterion*, Tunnelling and Underground Space Technology Vol. 15. No. 2, pp 187 – 213.

2 Panet, M. & A. Guenot 1982. *Analysis of convergence behind the face of a tunnel*, Tunnelling 1982, The Institution of Mining and Metallurgy, pp 197 - 204

3 Sulem, J., M. Panet & A. Guenot 1987. An Analytical Solution for Time-Dependant Displacements in a Circular Tunnel, Int. J. Rock Mech. Min. Sci. & Geomech. Abstr. Vol 24, No. 3, pp 155 - 164

4 Sellner, P. 2000. *Prediction of displacements in tunnelling*, PhD Thesis, Institute for Rock Mechanics and Tunnelling, Graz University of Technology.

5 Feder, G. & M. Arwanitakis 1976. *Zur Gebirgsmechanik ausbruchsnaher Bereiche tiefliegender Hohlraumbauten (unter zentralsymmetrischer Belastung)*, Berg- und Hüttenmännische Hefte, Jahrgang 121, Heft 4, pp 103 - 121

6 Schubert, P. 1988. *Beitrag zum rheologischen Verhalten von Spritzbeton*, Felsbau 6

7 Müller, M. 2001. *Kriechversuche an jungen Spritzbetonen zur Ermittlung der Parameter für Materialgesetze*, Diploma Thesis, Insitut für Gemoechanik, Tunnelbau und konstruktiven Tiefbau, Montanuniversität Leoben.

8 Committee CEN/TC 250 – SC (2005): *Eurocode 2 – Design of concrete structures – Part 1: General rules and rules for buildings*, European Committee for Standardisation